

# Theory and applications of the stress density

Alessio Filippetti<sup>1,2</sup> and Vincenzo Fiorentini<sup>1,3</sup>

(1) *Istituto Nazionale per la Fisica della Materia and Dipartimento di Fisica, Università di Cagliari, Italy*

(2) *Department of Physics, University of California, Davis, CA 95616, U.S.A.*

(3) *Walter Schottky Institut, Technische Universität München, Am Coulombwall, D-85748 Garching bei München, Germany*

(May 19, 2019)

Drawing on the theory of quantum mechanical stress, we introduce the stress density in density functional theory. In analogy with the Chetty-Martin energy density, the stress density provides a spatial resolution of the contributions to the integrated macroscopic stress tensor. We give specific prescriptions for a practical and efficient implementation in the plane wave ultrasoft pseudopotential method within the local-density approximation. We demonstrate the abilities of the stress density studying a set of representative test cases from surface and interface physics. In perspective, the stress density emerges as vastly more powerful and predictive than the integrated macroscopic stress.

68.35.-p,71.10-w,71.15.Mb

## I. INTRODUCTION

Energy and stress are quantities of obvious fundamental importance to the physics of solid state systems. In the last fifteen to twenty years, it has been possible to calculate them with progressively increasing accuracy from first-principles using density-functional theory (DFT).<sup>1</sup> The energy and stress as output from a typical calculation are a scalar and, respectively, a tensor whose values pertain to an entire finite system or to the unit cell of a periodic system. The relevance of the information they carry is concealed in their parametric dependence on external constraints, such as atomic geometries. It is not difficult, on the other hand, to picture situations in which access to local information related to energy or stress would be highly desirable. Clearly, such access would require a procedure allowing to sort out contributions to energy or stress due to specific regions inside the simulation cell.

By way of example, consider the calculation of the energy or stress change due to surface formation by means of the common repeated-slab supercell technique. The energy (or stress) of the slab contain several informations coupled to one another, which one would like to access separately. A simple case is that of a symmetric slab: to extract the properly surface-related quantities, the bulk contributions must be subtracted out, and this requires an independent bulk calculation. A qualitatively more complex case is that of an inherently asymmetric slab, such as frequently found in polar semiconductor surface simulations: in that case, two inequivalent surfaces are present, and their individual surface energies *cannot* be calculated independently. [It is occasionally possible to symmetrize the simulation cells in such a way as to obtain the surface energy of one of the surfaces, but even then only against a major computing effort.] Clearly, more basic issues may be addressed by a local energy or stress analysis: if a surface under stress reconstructs, and stress is the alleged driving force, it would be enlightening to know which parts of the systems tend to reduce rather

than increase their stress during the transformation.

Chetty and Martin,<sup>2</sup> looking for conceptual as well as practical solution to these and similar issues, introduced the energy density in the DFT framework. The energy density is a position-dependent density-functional scalar field whose integral upon the unit cell equals by construction the total energy. In general, this quantity is gauge dependent, *i.e.* not uniquely defined. Indeed, due to the long-range Coulomb interactions, the correspondence between a region of space and the energy stored therein is arbitrary, unless the value of the functional is fixed by symmetry at the boundaries of the region.

In an isolated system, the energy density is zero at the boundaries and outside, and the integral over the region enclosed by the boundaries is unique, and equals by construction the total energy. A more interesting situation where these requirements are satisfied is a surface (or interface) slab, infinite and periodic in the surface plane, and finite in the orthogonal direction. If its thickness is sufficient that bulk-like behavior is recovered in its interior, the energy associated with regions bounded by bulk layers is uniquely fixed and equal to the bulk energy (also relevant to the simple operative definitions<sup>3</sup> of surface energy). The vacuum contribution is zero by definition. Thus, the energy density in the surface regions obeys the appropriate boundary conditions, hence its integral upon that region is uniquely determined and gauge invariant. Similar arguments apply to interface slabs, that couple two different bulk regions and one (or quite possibly two, independent) interface region(s).

The concept of quantum-mechanical microscopic stress was introduced in the early days of quantum field theory,<sup>4</sup> and revisited and deeply investigated more recently.<sup>5–8</sup> In this paper, building upon the modern microscopic quantum-mechanical theory of stress<sup>6–8</sup> and drawing on the Chetty-Martin theory of the energy density,<sup>2</sup> we construct a position-dependent stress density. We start by defining the stress density as a rank-2 cartesian tensor field  $T_{\alpha\beta}(\mathbf{r})$  whose integral upon the cell equals by construction the macroscopic stress:

$$T_{\alpha\beta} = \int d\mathbf{r} \mathcal{T}_{\alpha\beta}(\mathbf{r}). \quad (1)$$

The formulation we present below is adapted to the practical plane-wave pseudopotential computational framework. The alternative definition of a stress field related to the force field  $F_\beta(\mathbf{r})$  through

$$F_\beta(\mathbf{r}) = -\nabla_\alpha \mathcal{S}_{\alpha\beta}(\mathbf{r}), \quad (2)$$

cannot be used in this framework, because it fixes  $\mathcal{S}$  only up to a gauge (the curl of an arbitrary function). While the gauge choice is unrestricted in principle, only the Maxwell gauge<sup>6</sup> is practically tractable for the stress field: that gauge satisfies Eq. (2) only for systems with purely coulombic interactions, conflicting with the fact that pseudopotentials produce non-coulombic interactions.

Numerous applications can be envisaged for the stress density. Those we focus on here concern surface and interface physics, as indeed structural instabilities and specific electronic effects at surfaces are fairly commonly associated with (among others) the surface excess stress.<sup>9</sup> Three point are worth some attention. First, a spatially-resolved stress function can be used to disentangle the macroscopic, integrated stress of inequivalent surfaces (or interfaces) that may be coupled into a single simulation cell, as is frequently the case for semiconductor polar orientations. Second, residual bulk contributions to the integrated stress can be computed from the stress density in the same calculation in a technically consistent fashion. Third, but definitely not least, the stress density can be applied as a “stress microscope” to investigate the role of stress in specific surface or interface processes; this kind of analysis, not relying merely on integrated macroscopic stress, can change *qualitatively* our understanding of the relation of surface stress with (e.g.) reconstruction<sup>10,11</sup> and adsorption.

The plan of the work is as follows: in Sec. II we formulate the stress density for density-functional theory in the local density approximation (LDA), for the specific instance of the plane-wave pseudopotential framework. In Sec. III we test the functionalities and accuracy of the stress density: specifically, in Sec. III A we apply it to the Al (111) surface, in Sec. III B to the the polar (100) and (111) surfaces of GaAs, and in Sec. III C to the (001) and (110) Ge/GaAs interfaces. Finally in Sec. III D we discuss an application of the stress density as a microscopic analysis tool in the case of metal surface reconstructions. Atomic units are used throughout.

## II. STRESS DENSITY FORMULATION IN DFT-LDA

Nielsen and Martin<sup>6</sup> carried out the quantum formulation of macroscopic stress for a general system of interacting particles. They also presented<sup>7</sup> an expression suitable

for the DFT-LDA framework, and the explicit form of the stress tensor for a plane-wave basis and pseudopotentials (a generalization exists<sup>12</sup> to gradient-corrected exchange-correlation functionals). An analogous formulation for an LCAO basis was provided by Feibelman.<sup>13</sup>

The Nielsen-Martin expression for the macroscopic stress is comprised of kinetic, exchange-correlation, electron-electron interaction, and electron-ion interaction term. For each of these contributions, we derive a space-resolved expression whose integral over the simulation cell equals the corresponding macroscopic quantity.

The macroscopic kinetic stress can be expressed in two equivalent ways, which reflect the gauge dependence of the kinetic stress density. The symmetric form is

$$T_{\alpha\beta}^{\text{kin}} = e^2 \sum_{\nu\mathbf{k}} f_{\nu\mathbf{k}} \omega_{\mathbf{k}} \int d\mathbf{r} \nabla_\alpha \psi_{\nu\mathbf{k}}^*(\mathbf{r}) \nabla_\beta \psi_{\nu\mathbf{k}}(\mathbf{r}), \quad (3)$$

and the antisymmetric form is

$$T_{\alpha\beta}^{\text{kin}} = -e^2 \sum_{\nu\mathbf{k}} f_{\nu\mathbf{k}} \omega_{\mathbf{k}} \int d\mathbf{r} \psi_{\nu\mathbf{k}}^*(\mathbf{r}) \nabla_\alpha \nabla_\beta \psi_{\nu\mathbf{k}}(\mathbf{r}), \quad (4)$$

where  $f_{\nu\mathbf{k}}$  and  $\omega_{\mathbf{k}}$  are occupation numbers and  $\mathbf{k}$ -point weights, respectively. The symmetric expression in Eq. (3) is preferable computation-wise as it does not involve second derivatives of the wavefunctions. Thus we define the kinetic stress density as

$$\mathcal{T}_{\alpha\beta}^{\text{kin}}(\mathbf{r}) = \frac{e^2}{2} \sum_{\nu\mathbf{k}} f_{\nu\mathbf{k}} \omega_{\mathbf{k}} [\nabla_\alpha \psi_{\nu\mathbf{k}}^*(\mathbf{r}) \nabla_\beta \psi_{\nu\mathbf{k}}(\mathbf{r}) + \text{c.c.}] \quad (5)$$

The calculation of  $\mathcal{T}_{\alpha\beta}^{\text{kin}}(\mathbf{r})$  is computationally inexpensive. The wavefunction derivatives are promptly calculated in Fourier space and then carried back to real space by fast-Fourier transform (FFT).

The exchange-correlation contribution to the macroscopic stress is

$$T_{\alpha\beta}^{\text{xc}} = -\delta_{\alpha\beta} \int d\mathbf{r} \rho(\mathbf{r}) [\epsilon_{xc}(\mathbf{r}) - V_{xc}(\mathbf{r})], \quad (6)$$

where  $\epsilon_{xc}$  and  $V_{xc}$  are the exchange-correlation energy density and the exchange-correlation potential, respectively, and  $\rho$  is the electronic charge density. The corresponding expression for the stress density follows straightforwardly:

$$\mathcal{T}_{\alpha\beta}^{\text{xc}}(\mathbf{r}) = -\rho(\mathbf{r}) [V_{xc}(\mathbf{r}) - \epsilon_{xc}(\mathbf{r})] \delta_{\alpha\beta}. \quad (7)$$

The macroscopic Hartree stress is given by

$$T_{\alpha\beta}^{\text{e-e}} = \frac{e^2}{2} \int \int d\mathbf{r} d\mathbf{r}' \rho(\mathbf{r}) \rho(\mathbf{r}') \frac{\partial}{\partial_{\alpha\beta}} \frac{1}{|\mathbf{r} - \mathbf{r}'|}$$

$$= -\frac{e^2}{2} \int \int d\mathbf{r} d\mathbf{r}' \rho(\mathbf{r}) \rho(\mathbf{r}') \frac{(r - r')_\alpha (r - r')_\beta}{|\mathbf{r} - \mathbf{r}'|^3}. \quad (8)$$

Due to the long-rangedness of coulombic interactions, there is no unique way to fix the stress density as a functional of the charge density. However, an optimal choice is the Maxwell gauge,<sup>2,6</sup> which is physically transparent and computationally easy to implement in our specific framework. The Maxwell stress density is

$$\mathcal{T}_{\alpha\beta}^H(\mathbf{r}) = -\frac{1}{4\pi e^2} [E_\alpha(\mathbf{r})E_\beta(\mathbf{r}) - \frac{1}{2}\delta_{\alpha\beta}E^2(\mathbf{r})], \quad (9)$$

where  $E_\alpha$  is the electric field

$$E_\alpha(\mathbf{r}) = -\nabla_\alpha \int d\mathbf{r}' \frac{\bar{\rho}(\mathbf{r}')}{|\mathbf{r} - \mathbf{r}'|}. \quad (10)$$

To cure the coulombic divergences in  $\mathcal{T}_{\alpha\beta}^H(\mathbf{r})$ , the total charge density

$$\bar{\rho} \equiv \rho^{\text{ion}} + \rho$$

should be used in Eq. (10), rather than the electronic charge density  $\rho$ . The ionic charge is represented by a sum of ion-centered Gaussians as

$$\rho^{\text{ion}}(\mathbf{r}) = -\sum_j \frac{Z_j}{\pi^{3/2} R_c^3} e^{-\frac{|\mathbf{r} - \mathbf{R}_j|^2}{R_c^2}}, \quad (11)$$

where  $\mathbf{R}_j$  and  $Z_j$  are ionic positions and charges, respectively, and  $R_c$  the gaussian radius. In this way  $\mathcal{T}_{\alpha\beta}^H$  contains the electron-electron interaction term,

$$-\frac{1}{4\pi e^2} [E_\alpha^{\text{e-e}}(\mathbf{r})E_\beta^{\text{e-e}}(\mathbf{r}) - \frac{1}{2}\delta_{\alpha\beta}E^{\text{e-e}2}(\mathbf{r})], \quad (12)$$

and the ion-ion interaction,

$$-\frac{1}{4\pi e^2} [E_\alpha^{\text{ion}}(\mathbf{r})E_\beta^{\text{ion}}(\mathbf{r}) - \frac{1}{2}\delta_{\alpha\beta}E^{\text{ion}2}(\mathbf{r})], \quad (13)$$

plus an unphysical term due to the fictitious interaction between electronic and Gaussian-ion charge density, to be taken care of below (see Eq. (17)). This procedure ensures charge neutrality within the volume bounded by bulk layers, besides that of the whole simulation cell. The crucial requirement that the stress density integral over

a bulk layer inside, *e.g.*, a surface slab to be equal to the bulk stress, is then satisfied. The electric field can be calculated in  $\mathbf{G}$ -space and then carried to real space where  $\mathcal{T}_{\alpha\beta}^H(\mathbf{r})$  is easily evaluated.

A further contribution to the ion-ion interaction arises from the strain derivative of the ionic charge density. In real space, this Ewald-like term reads

$$\mathcal{T}_{\alpha\beta}^{\text{Ewald}}(\mathbf{r}) = -\frac{R_c^2}{2} \nabla_\alpha \rho_j^{\text{ion}}(\mathbf{r}) E_\beta^{\text{ion}}(\mathbf{r}). \quad (14)$$

For a purely coulombic system, the previous formulas are all that is needed to construct the stress density. However, a practical implementation for the plane-wave pseudopotential method calls for several extensions, due mostly to the non-coulombic contributions of pseudopotential. The local pseudopotential stress contribution is

$$T_{\alpha\beta}^{\text{e-i}} = \int d\mathbf{r} \rho(\mathbf{r}) \sum_j \frac{\partial}{\partial \epsilon_{\alpha\beta}} V_j^{\text{loc}}(\mathbf{r} - \mathbf{R}_j), \quad (15)$$

where  $V_j^{\text{loc}}$  is the local part of pseudopotential sited on atom  $j$ . From  $\partial|\mathbf{r}|/\partial\epsilon_{\alpha\beta} = r_\alpha r_\beta/|\mathbf{r}|$ , it follows that

$$T_{\alpha\beta}^{\text{e-i}} = \sum_j \int d\mathbf{r} \rho(\mathbf{r}) V_j^{\text{loc}}(\mathbf{r} - \mathbf{R}_j) \frac{(r - R_j)_\alpha (r - R_j)_\beta}{|\mathbf{r} - \mathbf{R}_j|}, \quad (16)$$

where  $V_j^{\text{loc}}(x) = \partial V_j^{\text{loc}}(x)/\partial x$ . We define the corresponding stress density as

$$\mathcal{T}_{\alpha\beta}^{\text{e-i}}(\mathbf{r}) = \rho(\mathbf{r}) \sum_j \frac{\partial(V_j^{\text{loc}}(\mathbf{r}) + V_j^{\text{ion}}(\mathbf{r}))}{\partial\epsilon_{\alpha\beta}} \quad (17)$$

where the potential  $V_j^{\text{ion}}$  generated by the Gaussian ionic charges is added to compensate the same contribution present in Eq. (9), and to cancel the coulombic divergences in  $\mathcal{T}^{\text{e-i}}$ . The strain derivative of local pseudopotential in  $\mathbf{G}$ -space is (for brevity we use the same symbol for a quantity in  $\mathbf{G}$ - and  $\mathbf{r}$ -space)

---


$$\frac{\partial V_j^{\text{loc}}}{\partial \epsilon_{\alpha\beta}}(\mathbf{G}) = \sum_{\mathbf{G}' \neq 0} S_j(\mathbf{G}') \left[ \left( \frac{\partial V_j^{\text{loc}}(G')}{\partial G'^2} - \frac{4\pi e^2}{G'^4} \rho_j^{\text{ion}}(G') \right) 2 G'^\alpha G'^\beta + \left( V_j^{\text{loc}}(G') + \frac{4\pi e^2}{G'^2} \rho_j^{\text{ion}}(G) \right) \delta_{\alpha\beta} \right] \quad (18)$$

for all  $\mathbf{G} \neq 0$ , whereas the  $\mathbf{G} = 0$  contribution is

$$\frac{\partial V_j^{\text{loc}}}{\partial \epsilon_{\alpha\beta}}(0) = \left[ \alpha_j - \frac{\pi e^2 Z_j R_c^2}{\Omega} \right] \cdot \delta_{\alpha\beta} \quad (19)$$

Eq. (18) is derived using the fact that a positive strain  $\hat{\epsilon}$  in  $\mathbf{r}$ -space corresponds to linear order to  $\mathbf{G}' = (1 - \hat{\epsilon})\mathbf{G}$  in  $\mathbf{G}$ -space, thus

---


$$\frac{\partial V_j^{\text{loc}}}{\partial \epsilon_{\alpha\beta}}(\mathbf{G}) = -\frac{\partial V_j^{\text{loc}}}{\partial G^2} 2 G_\alpha G_\beta. \quad (20)$$

The  $\mathbf{G}$ -space derivative of  $V_j^{\text{loc}}$  is evaluated numerically.

The non local pseudopotential term only acts in the core regions, where spatial resolution is largely arbitrary. Therefore, we choose it to be a superposition of ionic-site centered contributions,

$$\mathcal{T}_{\alpha\beta}^{\text{nl}}(\mathbf{r}) = \sum_j P_{\alpha\beta}^j \delta(\mathbf{r} - \tau_j), \quad (21)$$

where stress

$$P_{\alpha\beta}^j = \sum_{\nu\mathbf{k}} f_{\nu\mathbf{k}} \omega_{\mathbf{k}} \langle \psi_{\nu\mathbf{k}} | \frac{\partial V_j^{\text{NL}}}{\partial \epsilon_{\alpha\beta}} | \psi_{\nu\mathbf{k}} \rangle \quad (22)$$

is the  $j^{\text{th}}$ -ionic site contribution. The most general form of a fully non local pseudopotential can be written as a non-diagonal projector

$$P_{\alpha\beta}^j = P_{\alpha\beta}^{j \text{ us}} + \sum_{\substack{\mathbf{k}, \mathbf{G}, \mathbf{G}' \\ \nu, n, m}} f_{\nu\mathbf{k}} \omega_{\mathbf{k}} D_{nm}^j e^{-i(\mathbf{G}-\mathbf{G}') \cdot \mathbf{R}_j} \psi_{\nu\mathbf{k}}^*(\mathbf{G}) \frac{\partial [\beta_n^j(\mathbf{k} + \mathbf{G}) \beta_m^j(\mathbf{k} + \mathbf{G}')]}{\partial \epsilon_{\alpha\beta}} \psi_{\nu\mathbf{k}}(\mathbf{G}'), \quad (24)$$

where

$$\frac{\partial \beta_n^j(\mathbf{k} + \mathbf{G})}{\partial \epsilon_{\alpha\beta}} = \frac{\partial \beta_n^j(\mathbf{k} + \mathbf{G})}{\partial (k + G)_\alpha} (k + G)_\beta. \quad (25)$$

The term  $P_{\alpha\beta}^{j \text{ us}}$  is only non-zero if ultrasoft pseudopotentials<sup>14</sup> are used. In that case,  $D_{nm}^j$  is non diagonal and contains a charge-dependent term,

$$D_{nm}^j = D_{nm}^0 + \int d\mathbf{r} Q_{nm}^j(\mathbf{r} - \mathbf{R}_j) [V^{\text{loc}}(\mathbf{r}) + V^{\text{Hxc}}(\mathbf{r})], \quad (26)$$

where  $V^{\text{Hxc}}$  is the screening (Hartree plus exchange-correlation) potential. The strain derivative of  $[V^{\text{loc}}(\mathbf{r}) + V^{\text{Hxc}}(\mathbf{r})]$  was already taken into account in Eq. (17), so the strain derivative of  $D_{nm}^j$  only contributes the term

$$P_{\alpha\beta}^{j \text{ us}} = \sum_{n, m, \mathbf{G}} B_{nm}^j e^{-i\mathbf{G} \cdot \mathbf{R}_j} (V^{\text{loc}} + V^{\text{Hxc}})^*(\mathbf{G}) \frac{\partial Q_{nm}(\mathbf{G})}{\partial \epsilon_{\alpha\beta}},$$

with

$$B_{nm}^j = \sum_{\nu\mathbf{k}} f_{\nu\mathbf{k}} \omega_{\mathbf{k}} \langle \psi_{\nu\mathbf{k}} | \beta_n^j \rangle \langle \beta_m^j | \psi_{\nu\mathbf{k}} \rangle. \quad (27)$$

The formulation of the stress density is now completed. The final expression reads

$$\begin{aligned} \mathcal{T}_{\alpha\beta}(\mathbf{r}) = & \mathcal{T}_{\alpha\beta}^{\text{kin}}(\mathbf{r}) + \mathcal{T}_{\alpha\beta}^{\text{H}}(\mathbf{r}) + \mathcal{T}_{\alpha\beta}^{\text{xc}}(\mathbf{r}) + \\ & \mathcal{T}_{\alpha\beta}^{\text{Ewald}}(\mathbf{r}) + \mathcal{T}_{\alpha\beta}^{\text{e-i}}(\mathbf{r}) + \mathcal{T}_{\alpha\beta}^{\text{nl}}(\mathbf{r}), \end{aligned} \quad (28)$$

the involved terms being given respectively by Eqs. (5), (7), (9), (14), (17), and (21). Operatively, all terms (except exchange-correlation) are first calculated in  $\mathbf{G}$ -space and then Fourier-transformed to  $\mathbf{r}$ -space, with a computational load comparable to that needed to calculate the macroscopic stress tensor. In order to accurately evaluate the stress density and the stress itself, a well-converged selfconsistent charge density is generally needed, due to the non-variational character of the stress, and its sensitivity to the details of the charge density.

$$V_j^{NL} = \sum_{nm} D_{nm}^j |\beta_n^j\rangle \langle \beta_m^j|, \quad (23)$$

where  $n, m$  are sets of atomic quantum numbers. In the case of ordinary Kleinman-Bylander pseudopotentials, the matrix  $D_{nm}^j$  is diagonal and its elements are constant, thus the corresponding stress is given by the strain derivatives of the projector functions  $\beta_n^j$ . In plane waves, we have in general

A practical point concerns how to handle and visualize the stress density (more discussion and examples are given in Sec. III). When dealing with surfaces and interfaces, appropriate averages of the stress density can be taken, that contain all the relevant information. If  $\hat{z}$  is the surface normal, the planar average is defined as

$$\begin{aligned} \overline{\mathcal{T}}(z) = & \frac{1}{A} \int dx dy \mathcal{T}(\mathbf{r}) \\ = & \delta_{G_x, 0} \delta_{G_y, 0} \sum_G \mathcal{T}(\mathbf{G}) e^{-iG_z \cdot \hat{z}}. \end{aligned} \quad (29)$$

A typical planar average (see Fig. 1) is strongly oscillating, with negative peaks at the ionic positions (corresponding mostly to attractive ion-electron contributions) and positive peaks in the interstitial region (corresponding mostly to kinetic compressive stress). Deviations from bulk-like behavior, signaling surface-induced stress changes, can be directly inspected. A further convenient way of analyzing  $\mathcal{T}(\mathbf{r})$  is its macroscopic average<sup>15</sup> over a period of length  $d$ , defined in turn as

$$\overline{\overline{\mathcal{T}}}(z) = \frac{1}{d} \int_{-d/2}^{z+d/2} dz' \overline{\mathcal{T}}(z'). \quad (30)$$

This filtering operation eliminates oscillations of period  $d$ , and can be generalized<sup>16</sup> to account for several superimposed oscillating components. If  $d$  is, e.g., the interlayer distance in a metal slab, then  $\overline{\overline{\mathcal{T}}}(z)$  is constant in the bulk region of the slab, and its value equals the bulk stress; in the vacuum region  $\overline{\overline{\mathcal{T}}}$  vanishes by construction. Any deviation from these constant values in the simulation cell quantify surface-related stress changes. In  $\mathbf{G}$ -space the macroscopic average reads

$$\overline{\overline{\mathcal{T}}}(G_z) = \frac{2}{d} \frac{\overline{\mathcal{T}}(G_z)}{G_z} \sin\left(\frac{d G_z}{2}\right), \quad (31)$$

where  $\overline{\mathcal{T}}(G_z) = \mathcal{T}(0, 0, G_z)$ .

### III. APPLICATIONS OF THE STRESS DENSITY

#### A. Non-polar surfaces: tests on Al (111)

To illustrate the basic characteristics of the stress density we first discuss the (111)-1  $\times$  1 surface of Al in the ideal (i.e. unrelaxed) structure. Calculations employed a 9-layers slab, norm-conserving pseudopotentials, and well converged plane-wave and k-point sets. In our formalism a negative stress is tensile, *i.e.* it indicates that reducing the interatomic distance is energetically favorable; a positive stress is compressive – that is, the system prefers to be stretched. The stress densities considered in the following are planar or macroscopic averages of the in-plane components  $\mathcal{T}_{xx}(\mathbf{r}) = \mathcal{T}_{yy}(\mathbf{r})$  (almost all the systems considered hereafter are isotropic in the surface plane): indeed, only the in-plane stress matters, since the orthogonal component is eliminated by relaxations.

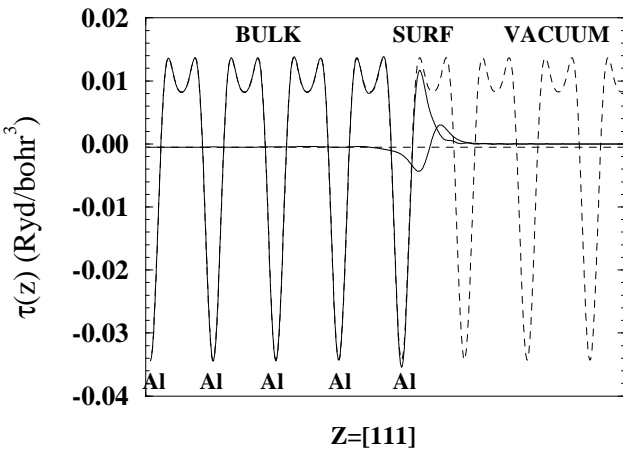


FIG. 1. Stress density of the unrelaxed Al (111) surface. Solid lines are planar and macroscopic averages for the surface slab, dashed lines same quantities for the bulk in the (111) slab symmetry (see discussion in text).

In Fig. 1 four curves are presented: two of them, the solid lines, are the planar and macroscopic averages of the stress density for the surface; the other two, the dashed lines, are the same quantities for the Al bulk in (111) symmetry (obtained filling up with atoms the vacuum region between repeated slabs). The comparison serves to better visualize changes due to the surface formation. Thanks to symmetry along [111], only half of the simulation cell is shown in Fig. 1.

As mentioned earlier, the planar averages are characterized by oscillations having the period of the interlayer distance in the bulk region. Negative peaks correspond to the layer positions by construction, and mostly store the tensile contribution due to the electron-ion interaction, whereas the positive peaks located between layers are dominated by compressive kinetic and coulombic terms. The surface planar average drops to zero on entering the

vacuum region, and it is informative to compare it with the bulk planar average near the surface.

The macroscopic average of the surface is constant in the bulk region and zero in vacuum, *i.e.* it is not constant only in the region where surface effects arise. Thus, it is enables one to identify the boundaries of the surface region. In the present case, for instance, the perturbation produced by surface formation extends roughly over one interlayer distance at the solid-vacuum interface. The macroscopic average for the bulk is everywhere constant, and it equals the surface macroscopic average in the bulk region. This common value of the two macroscopic averages in the bulk region, equaling by construction the bulk stress, is close but not equal to zero.

This is a first important capability of the stress density. It is a common feature of stress calculations that the stress be non-zero even though the lattice constant corresponds to theoretical equilibrium (hence in principle to zero stress). Indeed, energy minimization is usually performed at fixed plane-wave cutoff energy (*i.e.* variable number of plane-waves), whereas the stress is implicitly calculated at fixed number of plane waves.<sup>13,17</sup> This bias, specific of the plane-wave methodology, can be eliminated using an absolutely converged basis set, but that is highly impractical especially when dealing with large systems. Thus, the integrated surface stress should be obtained subtracting  $n$ -times the bulk contribution (if  $n$  is the number of atoms, or more generally of formula units, in the slab) from the total stress as

$$T_{\alpha\beta}^{\text{surf}} = \frac{1}{2} [T_{\alpha\beta}^{\text{slab}} - n T_{\alpha\beta}^{\text{bulk}}] \quad (32)$$

where factor 1/2 accounts for the two slab surfaces. As for the surface energies,<sup>3</sup> this procedure is justified in general to the extent that the finite-size basis error is proportional to the number of atoms, with the additional proviso that the error per atom does not change significantly for small changes in volume per atom.<sup>14</sup>

The stress density provides a straightforward evaluation of the spurious bulk stress, requiring no separate calculations, because the spurious bulk stress per atom is just the value of the macroscopic stress density average in the bulk region. Calculating the spurious stress in this fashion not only saves computing time, but also gives more accurate results, since use of the bulk stress calculated in the bulk unit cell in Eq. (32) introduces numerical errors beyond the basis-set error, due *e.g.* to inequivalent k-points. Another source of error is surface stress anisotropy (such as it occurs in most reconstructions): the spurious bulk stress is also expected to be anisotropic, a feature that cannot be but missed in the bulk unit cell.

Coming now to the shape of the macroscopic stress density average, we see that the surface formation causes an excess of tensile stress just below the surface-vacuum interface, partially compensated by an overshoot of compressive stress outside the interface. The resulting total surface stress is slightly tensile. The presence of tensile

stress is a common feature of most metal surfaces,<sup>18–20</sup> and its origin is easily understandable for *sp* metals<sup>20</sup> in terms of electron spill-out into vacuum, resulting in a reduction of the kinetic compressive stress in the near-surface region (the interpretation is slightly more involved<sup>18</sup> for transition metals). This tensile stress remains built-in at the surface, since surface atoms are constrained to their positions by the substrate potential, and in-plane contraction would require the formation of (typically costly) defects to be topologically possible.

We close this Section with an example of layer-by-layer resolution (LBL) of the stress. In Table I we list the LBL of the total stress for Al (111), i.e. the integrals of the planar stress density average over one interplanar distance. The 15 “geometrical” slab layers (9 are occupied by atoms) are labeled  $-7$  to  $7$ , layer 0 being the bulk-like slab center, and layers  $+n$  and  $-n$  being equivalent by inversion symmetry along  $\hat{z}$ . Layers  $-3$  to  $+3$  are bulk-like, having nearly equal LBL value. Their average stress ( $-0.743$  eV) equals to within 1 meV the bulk stress calculated in the bulk fcc. Inserting this value into Eq. (32) we obtain a value for the surface stress ( $-0.58$  eV/atom) unaffected by numerical errors. The resulting surface stress is in good agreement with the results of a similar procedure reported by Feibelman.<sup>19</sup>

### B. Polar surfaces: GaAs (100) and (111)

As briefly mentioned earlier, orientations for which cleavage produces inequivalent surfaces are a natural playground for the stress (and energy) density. We consider here two prototypical cases, namely the (100) and (111) surfaces of (zincblende) GaAs, which have been and still are the focus of intense experimental<sup>21–24</sup> and theoretical<sup>25–31</sup> work. These surfaces are polar, and present several (otherwise unpleasant) features making them suitable for a test of the stress density.

For the (100) orientation, each surface (Ga or As terminated) can indeed be individually simulated in a symmetric slab, so that the energy of each surface can be calculated via total energy differences; for testing purposes, however, we will also consider asymmetric slabs where inequivalent surfaces are coupled. For the (111) orientation, the surfaces are intrinsically different. Either are they geometrically identical but terminated by a different atom, or terminated with the same atomic species but with different geometries: the (say) Ga-terminated surfaces of a (111)-oriented slab are necessarily one (111) and one ( $\bar{1}\bar{1}\bar{1}$ ), and no symmetrization is practicable in this case. Using the energy density is then indispensable<sup>25–27</sup> for a direct calculation of the absolute surface energy of each surface, whereas only averages, or differences to some reference system are accessible by plain total energy calculations. The procedure is not straightforward, since it requires counting the atoms that belong to a given surface; this can be troublesome

for GaAs (111), and arguments based on cell symmetry adaptation<sup>25</sup> or space partitioning<sup>26</sup> have to be employed to complement the use of the energy density. Nevertheless, the energy density is more computationally convenient to study this surface than the total energy is.

Analogous considerations hold for the stress density, with the significant difference that there is no need to count surface atoms to evaluate the surface stress, and one need only making sure that the bulk structure is at theoretical equilibrium and the cutoff energy is large enough to render negligible the finite-size basis error.

There are other difficulties related to the presence of inequivalent surfaces. The two workfunctions are not lined up, and fictitious electric fields are produced in the vacuum region. Furthermore, as-cleaved GaAs (100) and (111) are metallic, because partially filled dangling-bond surface states are present on Ga- as well as As-terminated surfaces. As a consequence, a sizable charge transfer between the surface bands occurs across the slab; this artificial charge flow can be avoided resorting to passivation with, typically, fractionally charged H atoms. In reality these surfaces reconstruct into complex atomic arrangements to restore neutrality and remove metallicity; however, we decided to consider here only the unreconstructed and unpassivated surfaces, since they represent a technically intricate and critical case of supercell surface calculation if there ever was one, and are ideally suited as a testing ground for the stress density. We left the surfaces unrelaxed at the theoretical lattice constant.

Ga-terminated (Ga-t) and As-terminated (As-t) GaAs (100) can be represented individually within symmetric slabs. In this way, essentially no charge transfer across the slab occurs, barring the small residual interaction between surfaces which splits the (in principle degenerate) surface bands. On the other hand, the Ga-t and As-t surfaces can also be made to appear simultaneously in the same cell. This configuration is undesirable in general as it leads to sizable charge transfer, but it is useful as a test case; surface stresses obtained in the two symmetric (charge transfer unaffected) slabs can be directly compared with those of the coupled-surfaces asymmetric slab. For these  $1 \times 1$  surfaces we use 12 (plus 6 vacuum) layers for the asymmetric slab, 11 (plus 7) layers for the symmetric one. Ultrasoft pseudopotentials<sup>14</sup> are employed. The macroscopic averages are obtained by averaging over a distance of two interlayer spacings.

In Fig. 2 we show planar and macroscopic averages of the stress density in the asymmetric slab (solid lines), and the same quantities in the symmetric Ga-t slab (dashed lines). The macroscopic average inside the slab show that the bulk stress is zero to numerical accuracy, so that the surface stress is given directly by stress density integrals over one half of the slab. [Because the surfaces are non-stoichiometric, Eq. (32) cannot be used to eliminate the spurious bulk stress; we therefore had to use a sufficiently converged (60 Ryd cutoff) plane-wave basis so as to achieve a negligible residual bulk stress.] In the bulk region the averages for the symmetric and asym-

metric slabs are indistinguishable, indicating that in both structure the inner slab region is insensitive (stress-wise) to the surface. At the Ga-t surface the various averages match almost perfectly, indicating that the slabs are large enough to entirely decouple (stress-wise) the surfaces (mind that in one case the other surface is identical, in the other it is As-t). As expected, the calculated charge transfer is much larger for the asymmetric (0.02 electrons per cell, or  $5 \text{ mC/m}^2$ ) than for the symmetric slab ( $0.5 \text{ mC/m}^2$ ). The surface stress per surface cell obtained integrating the stress density upon the half slab containing the Ga-t surface is  $-1.114 \text{ eV/atom}$  per surface cell for the asymmetric slab, and  $-1.148 \text{ eV/atom}$  for the symmetric one. Thus the error due to charge transfer is about 3%, and well below 0.1 eV per surface cell, which is similar to that of half-slab integrals of the energy density in Ref. 2, where an analogous test was performed. Notice that for these unrelaxed structures the surface effects are very much localized on the surface atoms, and the bulk features are substantially recovered just one layer below the surface. Also, not surprisingly, the surface stress is tensile.

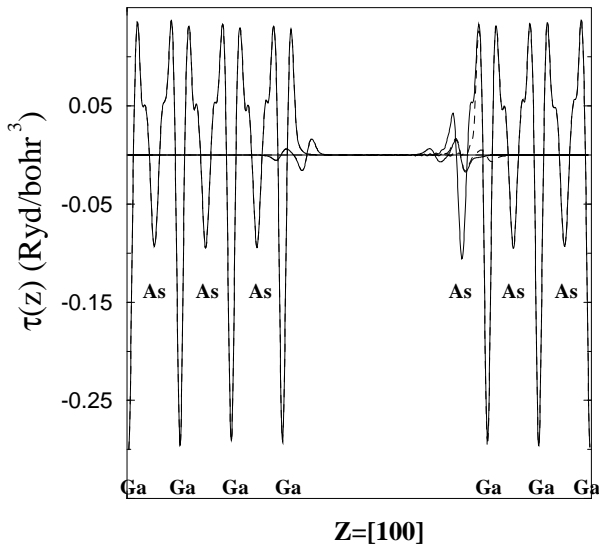


FIG. 2. Planar and macroscopic averages of the stress density for GaAs (100). Solid lines refer to the (asymmetric) slab containing both Ga-t and As-t surfaces, dashed lines to the symmetric slab for the Ga-t surface. Macroscopic averages vanish in the bulk and in the vacuum, and their integrals over the surface regions give the surface stresses. Solid and dashed lines are distinguishable only in the region of the As-t surface.

As already mentioned, for GaAs (111) there is no way to set up a symmetric slab containing only one kind of surface, since (111) and ( $\overline{1}\overline{1}\overline{1}$ ) surfaces are intrinsically different, and not related by any symmetry operation. We then we consider a comparison between the structure with both Ga-t and As-t (111) surfaces, and that one with Ga-t (111) and ( $\overline{1}\overline{1}\overline{1}$ ) surfaces (Fig. 3). The solid lines represent planar and macroscopic averages of the

slab with chemically different surfaces, the dashed ones are the analogous quantities for the Ga-t surface slab. Both the structures are now affected by an equal spurious charge transfer  $\sim 0.04$  electrons per cell; this is not unexpected since electron counting assigns in both cases the same occupation numbers to partially-filled surface bonds, that is,  $3/4$  on Ga-t (111) and  $1/4$  on As-t (111) and Ga-t ( $\overline{1}\overline{1}\overline{1}$ ). The comparison of the half-slab stresses containing the same Ga-t surface, *i.e.* the Ga-t surface stress, show an almost perfect agreement: we obtain  $-0.515 \text{ eV}$  for the same-ion surface slab, and  $-0.508 \text{ eV}$  for the different-ion surface slab. This is due both to the large number of bulk layers ensuring that there is no interaction between the surfaces in the slab, and to the (partially fortuitous) equality of charge transfer in the two slabs.

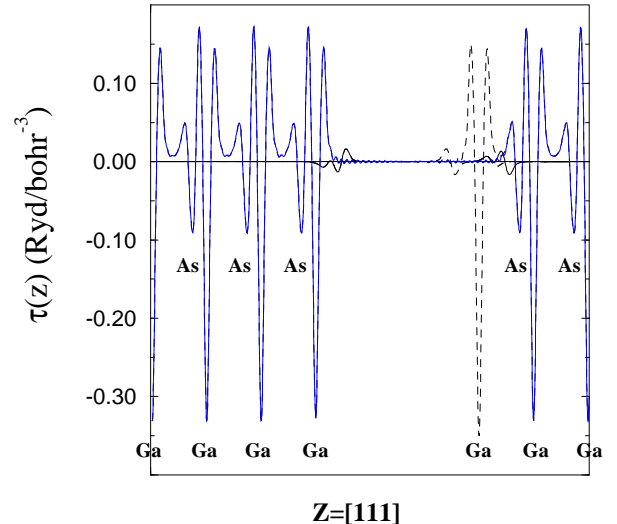


FIG. 3. Planar and macroscopic averages of stress density for GaAs (111). Solid lines refer to the slab with both Ga-t and As-t surfaces, dashed lines to that with (111) and ( $\overline{1}\overline{1}\overline{1}$ ) Ga-t surfaces.

### C. Ge/GaAs (100) and (110) interfaces

In this Section we present calculations on Ge/GaAs interfaces. For interfaces, the computing effort saved by using space-resolved quantities can be even higher than for the surfaces. First, the considerations of Sec. III B for polar surfaces apply in full also to inequivalent interfaces. Second, the simulation cell sizes are generally larger than for surfaces, hence the ability of avoiding separate calculations is very much welcome. Third, the relevant quantities entangled in the integrated stress (or energy) are at least three, namely the interface excess stress and the bulk stress of the two bulk phases, so that more separate bulk calculations are needed within the usual approach than in the surface case.

As an example of stress density application we first

present the case of the non-polar abrupt  $1 \times 1$  (110) Ge/GaAs interface. In Fig. 4, planar and macroscopic averages of the stress density are shown for a  $(\text{GaAs})_5(\text{Ge})_5$  slab. The in-plane lattice constant is fixed at the theoretical value for bulk GaAs; since the equilibrium lattice constant of bulk Ge is slightly larger, the Ge film is under tensile stress. The structure is unrelaxed, and the interlayer distances are those of bulk GaAs. [Note that these interfaces are stoichiometric, hence Eq. (32) can be used to get rid of the spurious bulk stress. The highly converged plane-wave basis used for the polar surfaces is not mandatory any more, and the cutoff was lowered to 25 Ryd. This produces an appreciable residual stress in GaAs.] The stress induced by the interface is barely visible in Fig. 4; only a small dip in the macroscopic average can be distinguished between the interface GaAs and Ge layers. For a non polar junction this is quite reasonable, since the charge transfer across the interface is too small and interface-localized to produce a significant excess stress. Integrating the planar (or macroscopic) average over the bulk regions we obtain  $T_{\text{bulk}}^{\text{GaAs}} = -0.94$  eV/atom and  $T_{\text{bulk}}^{\text{Ge}} = -1.52$  eV/atom. The resulting interface stress of  $T^{\text{int}} = 0.02$  eV/cell  $\sim 1$  meV eV/Å is practically vanishing. Clearly this nearly-matched interface is a test case where the stress due to the interface formation does not play any major role. Nevertheless, even in this case the power and semplicity of the stress density approach is evident.

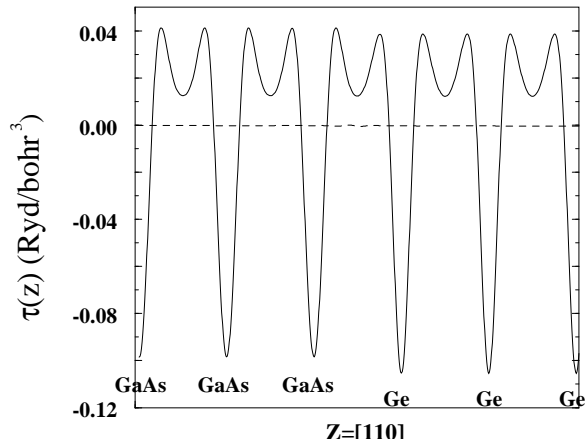


FIG. 4. Planar average (solid line) and macroscopic average (dashed line) of the stress density for the (110) Ge/GaAs interface. The presence of the interface is barely visible in the macroscopic average, since the interface is non polar and only very slightly mismatched. Only half slab is shown.

A more interesting case of interface-induced stress is illustrated in Fig. 5, where we show planar and macroscopic averages of the stress density for the mixed  $2 \times 1$  (100) Ge/GaAs interface. This polar interface is simulated with two bulk regions comprising 5 Ge and 5 GaAs layers, matched by a mixed Ga-Ge layer (12 layers and 24 atoms in total). The slab contains an equal number

of Ga and As atoms, so that the bulk GaAs contribution can be unambiguously subtracted out. It is also easily verified by the electron-counting rule<sup>32</sup> that no metallic states are present at the interface, which is in fact a reasonable candidate as the actual interface structure.

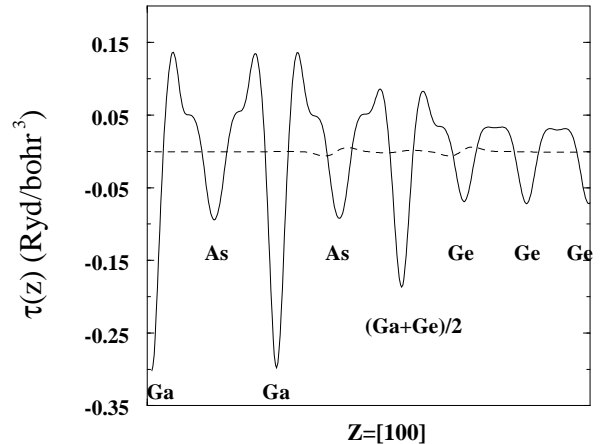


FIG. 5. Planar (solid line) and macroscopic (dashed line) average of the stress density for the mixed  $2 \times 1$  (100) Ge/GaAs interface. GaAs and Ge are interfaced by a mixed Ge/Ga layer. By symmetry, only one interface is shown.

The theoretical bulk GaAs in-plane lattice constant is imposed to the structure; the value of the macroscopic average in the bulk GaAs region represents just the finite-size basis error, whereas the bulk Ge region is also subject to strain. The bulk stresses are  $T_{\text{bulk}}^{\text{GaAs}} = -0.95$  eV/atom, and  $T_{\text{bulk}}^{\text{Ge}} = -1.61$  eV (the small differences from the values obtained in the (110) Ge/GaAs interface is due to k-point sampling). The interface region extends (stress-wise) over three layers, the mixed interface layer and the two adjacent to that. Outside this restricted region, the macroscopic average quickly recovers the equilibrium bulk value. The interface stress is 0.21 eV/atom, i.e. a condition of small compressive stress induced by the Ge epilayer.

#### D. Microscopic analysis based on the stress density

So far we have been giving examples of applications of the stress density to the calculation of macroscopic stress in cases where direct calculations would be troublesome. Actually, however, the stress density appears to be most useful in analyzing processes driven or simply influenced by the stress, as a kind of “stress microscope”. Reconstruction, adsorption, and growth are some of the phenomena in which stress can play a relevant role, possibly be a driving force, or simply function as a useful indicator of the ongoing processes.<sup>9,18</sup> The integrated stress, though, is sometimes of limited use, and occasionally misleading. While it does tell us whether the application of strain will be energetically favorable, it easily misses the

microscopic details, and cannot answer several legitimate questions such as: How far does the perturbation propagate below a surface or across an interfaces? How is the stress redistributed<sup>10</sup> into the perturbed region? What interplay of tensile and compressive contributions<sup>11</sup> produces the resulting integrated stress? Sometimes answering these questions is fundamental to attain a consistent qualitative view of a specific process, and indeed the stress density has been usefully applied in this fashion to the study of surface reconstructions.<sup>10,11</sup> Here, in particular, we discuss briefly the hex reconstruction of Ir (100), an apt example of what we mean by a microscopic analysis performed using stress density.

In this reconstruction, a quasi-hexagonal buckled layer (whereby 6 atoms take place into a  $5 \times 1$  surface area) is formed on top of the square (100) substrate. The increase in surface atomic density is expected to have a close relation to the surface stress, which is tensile and very large ( $-1.86 \text{ eV}/1 \times 1 \text{ area}$ ) on the unreconstructed surface. The easy guess (the “stress hypothesis”) would be that the densifying reconstruction is driven by the energy gained by partially or completely relieving the stress of the pristine surface. This hypothesis was indeed made plausible by comparing the stress-driven energy gain with model estimates of the substrate-surface rebonding cost, based *e.g.* on bond cutting arguments, or models of the defects needed to create the reconstruction.<sup>18,33</sup>

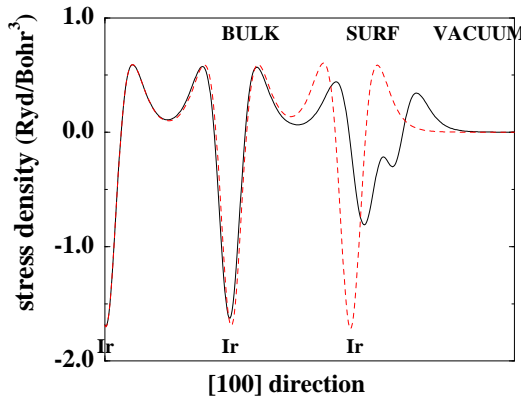


FIG. 6. Planar average of the stress density for unreconstructed (dashed line) and  $5 \times 1$ -reconstructed (solid line) Ir (100). The integrated stress is negative (i.e. tensile) for both the surfaces, and larger in magnitude for the reconstructed one.

The validity of previous models<sup>18,20,33</sup> does not depend on the value of the stress after the reconstruction; it is reasonable to assume, though, that the stress should decrease upon reconstruction, fittingly to its role of driving force. However, we found<sup>10,34</sup> that the surface tensile stress actually *increases* in magnitude by about 20% or  $0.3 \text{ eV}/1 \times 1 \text{ area}$  (on average on the  $\hat{x}$  and  $\hat{y}$  stress components of the anisotropic reconstructed surface) on Ir (001). Similar results are suggested by experiments<sup>35</sup> for Au (001). These new evidences on the integrated stress have increased the confusion, leading some to conclude<sup>35</sup>

that the “stress hypothesis” is invalid, *i.e.* that stress is not the driving force to reconstruction, and enhancing the mismatch between data and physical intuition. It turns out that the application of stress density<sup>11</sup> provides a natural explanation of the reconstruction mechanism, reconciling all previous theoretical and experimental observations.

In Fig. 6 the stress density planar average is shown for the (fully relaxed) reconstructed and unreconstructed (100) surfaces. Upon reconstruction the outermost negative and two outermost positive peaks, storing tensile and compressive contribution, respectively, are strongly reduced. The surface layer relaxes outwards by a huge 20% of the ideal interplanar distance, which is also reflected in the outward shift of the tensile peak. The smearing of the latter is a token of the large surface buckling. From these findings, the following picture readily emerges. The decreased interatomic distance in the surface layer correlates with the severe reduction of the tensile stress within that layer (suppression of tensile peak). At the same time, the surface layer needs to relax outward to reduce its interaction with the substrate potential; this displacement correlates with the decrease of the compressive (kinetic) contribution to the stress, because more room is provided to the electronic charge to delocalize in between the top surface layers. Thus the net negative change of total surface stress (more tensile after reconstruction) results from the competing reductions of tensile and compressive contributions that are easily related to structural changes. In particular, while the pre-existing tensile stress can be clearly identified as driving force, the change in compressive stress resulting from the surface rearrangement to accommodate the surface-substrate mismatch can be interpreted as a residual “resisting” force of the substrate. The post-reconstruction stress contains both contributions, inextricably entangled. It appears that the conclusion drawn from the post-reconstruction total stress, that the transition is not-stress driven, is incorrect. Further details on this reconstruction can be found elsewhere.<sup>10</sup>

One may object to this usage of the stress density on grounds that the shape of the stress density as a function of the space coordinates is arbitrary, and fixed by gauge. This limitation is indeed more academic than practical: although the detailed shape of the stress density does depend on the gauge, the stress density change due to a perturbation in a given system for a given gauge is expected to be essentially gauge-independent. Hence, analyzing stress density changes upon reconstruction (or adsorption, etc.) is sensible and meaningful.

#### IV. SUMMARY

Drawing on the theory of quantum mechanical stress, we introduced the stress density in density functional theory, giving specific prescriptions for a practical and effi-

cient implementation for the plane wave ultrasoft pseudopotential method within the local-density approximation. In analogy with the Chetty-Martin energy density, the stress density provides a spatial resolution of the contributions to the integrated macroscopic stress tensor. We applied the newly introduced concept to a wide-ranging set of test cases selected from surface and interface physics. It is appropriate to point out that in this paper we gave just a flavor of the possible applications, that are far from being exhausted by those presented here. In perspective, the stress density is way more powerful and predictive than the integrated macroscopic stress, and opens up new ways towards an understanding of the physics of stress-driven phenomena.

## ACKNOWLEDGMENTS

Calculations were performed mostly on the late IBM SP2 of CRS4, Cagliari. VF was supported by the Alexander von Humboldt-Stiftung during his stay at the WSI.

- <sup>1</sup> R. M. Dreizler and E. K. U. Gross, *Density Functional Theory* (Springer, Berlin 1988).
- <sup>2</sup> N. Chetty and R. M. Martin, Phys. Rev. B **45**, 6074 (1992).
- <sup>3</sup> V. Fiorentini and M. Methfessel, J. Phys.: Cond. Matt. **8**, 6525-6529 (1996).
- <sup>4</sup> E. Schrödinger, Ann. Phys. (Leipzig) **82**, 265 (1927); W. Pauli, in *Handbuch der Physik, Band XXIV, Teil 1* (Springer, Berlin, 1933), pp. 83-272; Vol. V, Part 1 (1958); P. C. Martin and J. Schwinger, Phys. Rev. **115**, 1342 (1959); A. Kugler, Z. Phys. **198**, 236 (1967).
- <sup>5</sup> O. H. Nielsen and R. M. Martin, Phys. Rev. Lett. **50**, 697 (1983).
- <sup>6</sup> O. H. Nielsen and R. M. Martin, Phys. Rev. B **32**, 3792 (1985).
- <sup>7</sup> O. H. Nielsen and R. M. Martin, Phys. Rev. B **32**, 3780 (1985).
- <sup>8</sup> N. O. Folland, Phys. Rev. B, **34** 8296 (1986); **34** 8305 (1986).
- <sup>9</sup> H. Ibach, Surf. Sci. Rep. **29**, 193 (1997).
- <sup>10</sup> A. Filippetti and V. Fiorentini, to be published.
- <sup>11</sup> A. Filippetti and V. Fiorentini, to be published.
- <sup>12</sup> A. Dal Corso and R. Resta, Phys. Rev. B **50**, 4327 (1994).
- <sup>13</sup> P. J. Feibelman, Phys. Rev. B **50**, 3916 (1991).

- <sup>14</sup> K. Laasonen, A. Pasquarello, R. Car, Changyol Lee, and D. Vanderbilt, Phys. Rev. B **47**, 10142 (1993).
- <sup>15</sup> A. Baldereschi, S. Baroni, and R. Resta, Phys. Rev. Lett. **61**, 734 (1988);
- <sup>16</sup> L. Colombo, R. Resta, and S. Baroni, Phys. Rev. B **44**, 5572 (1991).
- <sup>17</sup> R. D. Meade and D. Vanderbilt, in *Proceedings of the Materials Research Society*, edited by J. Tersoff, D. Vanderbilt and V. Vitek (Material Research Society, Pittsburgh, PA, 1989), p. 451.
- <sup>18</sup> V. Fiorentini, M. Methfessel, and M. Scheffler, Phys. Rev. Lett. **71**, 1051 (1993).
- <sup>19</sup> P. J. Feibelman, Phys. Rev. B **50**, 1908 (1994); Phys. Rev. B **51**, 17867 (1995).
- <sup>20</sup> R. J. Needs, M. J. Godfrey, and M. Mansfield, Surf. Sci. **242**, 215 (1991).
- <sup>21</sup> C. Messmer and J. C. Bilello, J. Appl. Phys. **52**, 4623 (1981).
- <sup>22</sup> W. Weiss *et al.*, Surf. Sci. **221**, 91 (1989).
- <sup>23</sup> D. K. Biegelsen *et al.*, Phys. Rev. Lett. **65**, 452 (1990).
- <sup>24</sup> R. Nötzel *et al.*, Phys. Rev. B **46**, 4736 (1992).
- <sup>25</sup> N. Chetty and R. M. Martin, Phys. Rev. B **45**, 6089 (1992).
- <sup>26</sup> K. Rapcewicz, B. Chen, B. Yakobson, and J. Bernholc, Phys. Rev. B **57**, 7281 (1998).
- <sup>27</sup> N. Moll, A. Kley, E. Pehlke, and M. Scheffler, Phys. Rev. B **54**, 8844 (1996).
- <sup>28</sup> E. Kaxiras *et al.*, Phys. Rev. B **35**, 9625 (1987); Phys. Rev. B **35**, 9636 (1987).
- <sup>29</sup> G. Quian, R. M. Martin and D. J. Chadi, Phys. Rev. B **37**, 1303 (1988); Phys. Rev. B **38**, 7649 (1988).
- <sup>30</sup> T. Ohno, Phys. Rev. Lett. **70**, 631 (1993).
- <sup>31</sup> J. E. Northrup and S. Froyen, Phys. Rev. Lett. **71**, 2276 (1993); Phys. Rev. B **50**, 2015 (1994).
- <sup>32</sup> J. A. Appelbaum, G. A. Baraff, and D. R. Hamann, Phys. Rev. B **14**, 1623 (1976).
- <sup>33</sup> S. Oppo and V. Fiorentini, Phys. Rev. Lett. **81**, 4278 (1998).
- <sup>34</sup> A. Filippetti and V. Fiorentini, Surf. Sci. **377**, 112 (1997).
- <sup>35</sup> C. E. Bach, M. Giesen, H. Ibach, and T. L. Einstein, Phys. Rev. Lett. **78**, 4225 (1997).

TABLE I. Layer-by-layer (LBL) decomposition of the integrated stress for an Al (111) surface slab. The slab is built up by 15 (9 atomic plus 6 vacuum) layers, labeled from  $-7$  to  $+7$ . Layer 0 is the bulk-like slab center, and  $+n$  and  $-n$  layers are identical by symmetry. Values are in eV/atom.

	0	$\pm 1$	$\pm 2$	$\pm 3$	$\pm 4$	$\pm 5$	$\pm 6$	$\pm 7$
$T^{\text{LBL}}$	-0.779	-0.734	-0.706	-0.771	-2.059	0.729	0.0	